

**Photoexcited *trans*-polyacetylene, poly(*p*-phenylene vinylene) and carbyne chains
in amorphous hydrogenated carbon probed by resonant Raman scattering**

M. Rybachuk ^{1,2*} and J.M. Bell ²

¹ *Federal Institute for Materials Research and Testing (BAM), Division VI.4 Surface
Technology, Unter den Eichen 87, 12205 Berlin, Germany*

² *Faculty of Built Environment and Engineering, Queensland University of
Technology, 2 George St, Brisbane, Qld 4001, Australia*

Receipt date:

PACS codes: 81.05.Uw, 78.30.Ly, 61.43.Dq, 61.41.+e

Abstract

Inclusions of carbyne, *trans*-polyacetylene [*trans*-(CH)_x] and poly(*p*-phenylene vinylene) (PPV) chains is revealed via the resonant Raman scattering (RRS) investigation of amorphous hydrogenated carbon (*a*-C:H) films in N-IR – UV range. The RRS spectra of *trans*-(CH)_x core A_g modes (C-C at 1060 cm⁻¹ and C=C at 1450 cm⁻¹ in N-IR) and PPV CC-H phenylene group mode at *ca.* 1175 cm⁻¹ were found to transform and disperse as the laser excitation energy $\hbar\omega_L$ is increased from N-IR through visible to UV, whereas carbyne inclusions only become evident in UV. In

view of this effect, the RRS spectral features are attributed to $\hbar\omega_L$ selective probing of $trans-(CH)_x$ chain inhomogeneity and the distribution of chains with varying length of π - electron conjugation, while for PPV these features are attributed to the resonant probing of phenylene ring disorder; and for sp segments, to enhanced probing of a local band gap of end-terminated polyynes by excitation energy. The infra-red analysis confirmed the presence of sp -hybridised, $trans-(CH)_x$ and PPV inclusions. The obtained RRS results for a -C:H denote differentiation between the core A_g $trans-(CH)_x$ modes and the PPV phenylene mode. It was also found that the response of $trans-(CH)_x$ segments included into an amorphous carbon matrix to changing $\hbar\omega_L$ is identical to of free-standing chains in the neutral bulk $trans$ -polyacetylene. The latter finding can be used to facilitating identification of $trans-(CH)_x$ in complex carbonaceous materials spectra.

I. INTRODUCTION

Amorphous carbon (*a*-C) and diamond-like carbon (DLC) solids are characterised by a large variety of types and properties that stem from combinations of principally two hybridised forms of carbon sp^2 and sp^3 and, for carbon solids formed in presence of hydrogen, as for *a*-C:H, the resultant properties are also controlled by the hydrogen content. Isotropic solids like DLC or *a*-C can, in principal, contain inclusions of a basic polymer, the *trans* isomer of polyacetylene [*trans*-(CH)_x] according to simulations by Bernasconi *et al.*¹ This introduced the idea that C–C bonds in bulk *trans*-(CH)_x undergo a gradual saturation via chain interlinking at high pressure, transforming into an *a*-C:H solid, and earlier experiments by Arbuckle *et al.*² showing that sp^3 clustering occurs if defect concentrations in *trans*-(CH)_x reach sufficiently high level. These findings can be related to the energetic mechanism of sp^2 and sp^3 bonding formation in a hydrogenated DLC.³ The presence of *trans*-(CH)_x in a carbonaceous solid was reported by López-Ríos *et al.*⁴ for CVD synthesised diamond, and Dischler *et al.*⁵ and Piazza *et al.*⁶ identified *trans*-(CH)_x inclusions in low temperature synthesised *a*-C:H. Assignment of a Raman peak at *ca.* 1140 cm⁻¹ to ω_1 C–C in plane bending mode and a peak at *ca.* 1490 cm⁻¹ to ω_3 C=C stretching mode to those of *trans*-(CH)_x was, at first, uncertain, since solution synthesised *trans*-(CH)_x is known to be unstable at the elevated temperatures used in ordinary DLC deposition.^{4, 7, 8} Some authors inferred that very short (less than 20 C=C units) temperature stable *trans*-(CH)_x segments are formed between the diamond grains during deposition.^{4, 9, 10} Isotopic substitution experiments⁴ by Kuzmany *et al.*¹¹ and Michaelson *et al.*¹² confirmed the assignment of the ω_1 and ω_3 modes to *trans*-(CH)_x. Recently Teii *et al.*¹³ made an effort to correlate the interaction between the hydrogen-

rich plasma and the amount of *trans*-(CH)_x in nanocrystalline diamond films. Conclusive results, however, were not obtained since at present, the means to quantitatively identify the amount and/or the ordering of *trans*-(CH)_x inclusions in a given *a*-C or DLC solid are not sufficiently defined.

The purpose of this work is to present the resonant Raman scattering (RRS) investigation of basic *a*-C:H films in the N-IR – UV range, and to demonstrate that these films host *trans*-(CH)_x inclusions (chains) characterised by intrinsic ordering and variable conjugation length; and to show that films also contain carbyne chains and inclusions of poly(*p*-phenylene vinylene) (PPV).¹⁴ The carbyne species considered are short hydrogen-terminated polyynes chains. Here we obtain experimental and theoretical results that demonstrate differentiation between Raman modes of *trans*-(CH)_x (core *A_g* modes) and the PPV phenylene mode in *a*-C:H. We illustrate that the Raman response of core *A_g* *trans*-(CH)_x modes included into an *a*-C:H solid, when probed by varying Raman excitation energies ($\hbar\omega_L$), conforms to the classical behaviour of isolated, free-standing *trans*-(CH)_x chains, showing the strong change in the shape of the most intense bands in the spectra depending on the excitation energy as illustrated in Fig. 1 for different excitation laser wavelengths, ω_L .¹⁵ That is, ω_1 and ω_3 *trans*-(CH)_x modes in *a*-C:H spectra become transformed and change position, (dispersion⁹), shape and intensity with changing $\hbar\omega_L$, and this transformation depends on the inherent degree of inhomogeneity of *trans*-(CH)_x chains. The distribution of *trans*-(CH)_x segments with varying degrees of inhomogeneity (conjugation chain length, bond disorder) was computed employing the bi-modal chain distribution model proposed by Brivio and Mulazzi *et al.*^{8, 15, 16} and the amplitude mode theory proposed by Ehrenfreund *et al.*⁷. We aim to elucidate a simple approach that is needed

to facilitate extraction of $trans\text{-(CH)}_x$ contributions from the core $a\text{-C}$, DLC or any spectra where $trans\text{-(CH)}_x$ contributions could be clearly observed.

The RRS has been successfully used to study inhomogeneity and disorder in amorphous carbon systems consisting of arbitrary combinations of sp , sp^2 and sp^3 hybridised states.^{3, 7, 9, 17-19} In this work the excitation energies over a wide range of energies from 1.58 eV to 5.08 eV were used, ensuring that the vibrational density of states (VDOS) of the great majority of sp^3 , sp^2 and sp carbon mixtures are measured. The chance of sp carbon allotrope formation as either polyynes ($\text{-C}\equiv\text{C-}$)_n, a semiconductor, or polycumulene (=C=C=)_n, a semi-metal²⁰, in an energetic hydrogenated environment is very low, considering that both species are highly unstable to hydrogen exposure²¹ and temperature sensitive.^{5, 22, 23} Identification of carbyne inclusions in the hydrogenated $sp^2\text{-}sp^3$ aggregates are therefore, highly notable, since the sp self-organisation mechanism, even at present, remains largely unresolved.²⁴⁻²⁸ We focused on detection of sp -hybridised segments using RRS process, and critically consider recent findings by D'Urso *et al.*¹⁹ In addition, infra-red absorption spectra analysis was used to identify sp and $trans\text{-(CH)}_x$ species.

II. EXPERIMENTAL

Deposition of $a\text{-C:H}$ films were performed on Si $\langle 111 \rangle$ wafers using a Helmholtz-type inductively coupled plasma (ICP) reactor operated on CH_4/Ar mixture at temperatures of 380 – 400 K.^{29, 30} The pressure was 6 (10^{-2} Pa) and the substrate was DC negatively biased at -250 to -300 V. The use of substrate bias this range was found to have adverse effects to the formation of sp or $trans\text{-(CH)}_x$ segments. The

formation of *trans*-(CH)_x and *sp* bonded segments appears to be facilitated by the amount of atomic hydrogen³¹ in hydrocarbon plasma, and the ratio of 55 % CH₄ to 45 % Ar was found to be most favourable in this work. Deposition was performed at extremely low rate of ~30 nm/hour in a high density plasma, with the aim of obtaining high ordering of *sp*² phase, and allowing for a higher concentration of free radicals and a higher degree of gas phase reaction taking place.

The fabricated films were found to be of low stress ≤ 1 GPa, with hardness of approximately 20 GPa and a friction coefficient of 0.07 at 70 % humidity measured by a nano-mechanical testing (UMIS). Electrical resistivity was ≥ 8 ($10^8 \Omega \text{ cm}$) measured by using a four-probe testing method. Films were ~140 nm thick with a maximum refractive index of 2.2 in the UV–blue region, as measured by IR – UV spectroscopic ellipsometry (J. A. Woollam Co.). The hydrogen content in the films was determined from the analysis of infra-red absorption spectra as used by Liu *et al.*³² (normal mode vibrational frequency calculations) and from the analysis of UV Raman spectra (ω_L of 244 nm) as proposed by Casiraghi *et al.*³³ where the full width at half maximum (FWHM) of the G peak, G peak position and the dispersion of this peak at respective $\hbar\omega_L$ were used. This gave a hydrogen content of approximately 27 (± 2.5) at%.

The infra-red (IR) spectra in the range 3400 – 2600 cm^{-1} range were obtained using Nicolet Nexus Fourier transform infra-red (FT – IR) spectrometer operated in transmission mode with subtraction of Si substrate background. For IR measurements, the same group (thickness, lattice orientation, and surface finish grade and backside surface roughness) of uncoated Si substrates was used, as for the film deposition experiments. Standard Gaussian peak functions were used to fit the constituent bands in the selected spectral range after linear background subtraction.

Analysis of X-ray core C_{1s} and valence bands photoelectron spectra obtained using Kratos Axis Ultra instrument fitted with a monochromated $Al K_{\alpha}$ 1486.6 eV x-ray source determined the sp , sp^2 and sp^3 contents to be 3 %, 67 % and 30 % respectively with an uncertainty of less than 1.25 %. The sp -hybridized content was verified by analysing 244 nm Raman^{19, 34, 35} and infra-red⁵ results, and the sp^3 content using 244 nm Raman results^{17, 33}.

Unpolarised Raman spectra across the excitation energy range 5.08 eV to 1.28 eV were obtained *ex situ* at 293 K using 244, 532, 633, and 785 nm Renishaw instruments and 325 and 442 nm Kimmon Raman instruments. All excitation wavelengths excluding 785 nm were pulsed; the 785 nm was a continuous wavelength laser source. The frequency-doubled *Ar* ion laser was used for 244 nm, *He/Cd* for 325 and 442 nm, the frequency-doubled YAG laser was used for 532 nm, *He/Ne* gas laser was used for 633 nm, and a diode laser source was used for 785 nm excitations. All measurements were taken in dynamic mode with a specimen moved linearly at speeds of up to 30 m/s and laser power was kept at or below 1 mW for all wavelengths minimizing the thermal damage. The acquisition time was varied between 10 s to 120 s and the spectral resolution was 1 cm^{-1} .

There were two main options for fitting of the Raman spectra as noted by Casiraghi *et al.*³³: an all Gaussians fit to Raman constituent bands, or a fit with a Breit–Wigner–Fano (BWF) line shape³⁶ for the *G* peak and a Lorentzian for the *D* peak. The *a*-C:H samples selected for this study did not display significant photoluminescence (PL) background, nonetheless, we find that the use of the BWF line is not the most appropriate since the BWF Q coupling coefficient is influenced by the PL background, and the BWF lineshape tends to adjust its asymmetry reproducing a part of the PL slope.^{33, 36} This does not lead to reproducible fitting of the Raman

spectra. Alternatively, fully symmetric Gaussian line-shapes provide better, reproducible fit in the presence of a PL background. In the Raman spectra presented, the linear PL background was subtracted and all constituent peaks were fitted with Gaussian line-shapes using a nonlinear least squares fitting procedure.³⁷

III. RESULTS AND DISCUSSION

A. Identification of π - conjugated polymeric inclusions in *a*-C:H

Figure 2 shows the RRS spectra of an examined *a*-C:H film with PL background subtracted and fitted with Gaussian line-shapes to the constituent peaks. The fitted bands are common DLC *D* and *G* modes for N-IR and visible and the *T* mode for UV $\hbar\omega_L$ excitations¹⁷; and the two A_g zone center vibrational modes of *trans*-(CH)_x, the ω_1 and ω_3 .^{7, 18, 38} The weak ω_2 mode that usually appear at 1275 – 1295 cm⁻¹ range (a peak labelled '1294', Fig. 1) was not present, nor the peak corresponding to the B_g mode of *trans*-(CH)_x that is normally observed in 1000 - 1100 cm⁻¹ range (a peak labeled '1020', Fig. 1), however their contributions could be hidden by the tails of the fitted *D* and the ω_1 bands. Fundamentally, the absorption for free-standing *trans*-(CH)_x occurs within 1.5 - 1.7 eV range and corresponds to the zone centre A_g Raman modes at opening frequencies of 1060, 1280 and 1450 cm⁻¹.^{18, 38} That is at N-IR $\hbar\omega_L$. As the Raman excitation energy increases, and therefore moves away from the band gap resonance, the Raman sidebands exhibit radical lineshape changes as illustrated in Fig. 1.^{15, 18, 39, 40} Shoulders appear at the high frequency side of the primary ω_1 and ω_3 modes that eventually extend into secondary peaks at excitation energies well above

the band gap at $\hbar\omega_L = 2.71$ eV.¹⁸ The RRS spectra disperses⁹ and the resultant *trans*-(CH)_x peaks change intensities, I and widths Γ , and the overall spectrum is in addition affected by light polarisation.^{41, 42} The RRS of *trans*-(CH)_x secondary peaks, such as the peaks appearing at ω_L of 457.9 nm (noted as '1126' and '1500', Fig. 1) in free-standing samples become more pronounced at higher excitation energy. However, the complexity of separating *trans*-(CH)_x from the host DLC modes leads us to analyse a single symmetric band distribution.³⁹ This approach was proved by Ehrenfreund *et al.*⁷ to be sufficient to account for a double peak Raman structure.

Together with common DLC and *trans*-(CH)_x modes we find a peak positioned at 1175 cm⁻¹ when probed by 785 nm ω_L which we assign to a *CC-H* bending mode of the ring in neutral poly(*p*-phenylene vinylene) (PPV).^{43, 44} The origin of this mode could, in fact, be due to defects in *sp*² aromatic rings since in single crystals, only phonons with the wave vector rule $k=0$ contribute to Raman scattering. Defects lead to relaxation of this selection rule and therefore provide means for phonons from outside the centre of the Brillouin zone to contribute to the Raman scattering. If this 1175 cm⁻¹ mode indeed belongs to PPV chains, the other PPV zone centre vibrational modes found at higher frequencies in 1200 – 1330 and 1540 – 1625 cm⁻¹ range will certainly be obscured by the host *D* and the *G* modes.⁴⁵ Owing to its large width, Γ_{1175} the 1175 cm⁻¹ vibrational mode could be effectively a combination of vinylene and a *CC-H* ring bend modes since the zone mode frequency for vinylene is at approximately 1145 cm⁻¹.⁴³ As the Raman excitation energy increases from N-IR to UV range all peak positions shift to a higher vibrational frequency obeying phonon confinement rules¹⁷, as shown in Fig. 3(a) where peak dispersion, $\Delta\omega$ is denoted as the shift in a peak position relative to base position at N-IR excitation ($\hbar\omega_L=1.58$ eV). Fig. 3(b) summarizes changes in widths for all fitted peaks.

The gradual decrease in $I(D)/I(G)$, the intensity ratio for the D and G peaks, from ~ 0.9 to 0.2 , the pronounced reduction in Γ_D and Γ_G , and the G peak saturating¹⁷ at approximately 1590 cm^{-1} for 244 nm excitation indicate that $a\text{-C:H}$ films hosting $trans\text{-(CH)}_x$ and PPV inclusions consist of a highly ordered and symmetric sp^2 phase.^{17, 30} There is no T peak dispersion at higher excitation energies in agreement with earlier reports.¹⁷ The band gap for PPV is in the range of $2.2 - 2.5 \text{ eV}$ ^{44, 46} and therefore it is selectively probed by excitation energy corresponding to green light (ω_L of 532 nm). Figure 4 illustrates relative changes of the fitted ω_1 , ω_3 and 1175 cm^{-1} bands in the spectra of $a\text{-C:H}$ as a function of $\hbar\omega_L$.

Fig. 5(a) illustrates changes in the relative intensity of the 1175 cm^{-1} peak, $I(1175)$ at different excitation energies; $I(1175)$ is calculated as intensity of the 1175 peak over the total intensity of all constituent peaks including the intensity of the T peak in the UV Raman spectra. The $I(1175)$ reaches its highest intensity position at $\hbar\omega_L=2.3 \text{ eV}$ as revealed in Fig. 4, although Fig. 3(b) shows that changes in the peak width, Γ_{1175} are minor at this band gap frequency. This PPV peak at 1175 cm^{-1} is certainly of sp^2 origin since its contributions disappear in UV excitation.

The total relative intensity for $trans\text{-(CH)}_x$ contributions calculated as sum of relative intensities of ω_1 , $I(\omega_1)$ and ω_3 , $I(\omega_3)$ peaks and denoted as $I\Sigma(\omega_1, \omega_3)$ is shown in Fig. 5(a). The magnitude of $I\Sigma(\omega_1, \omega_3)$ gradually decreases from N-IR to UV $\hbar\omega_L$. Individual trends of $I(\omega_1)$ and $I(\omega_3)$ contributions are shown in Fig. 4 and Fig. 5(b). The $trans\text{-(CH)}_x$ features as $I(\omega_1)$ and $I(\omega_3)$ intensities (Fig. 4 and Fig. 5(b)) and peak widths, Γ (Fig. 3(b)) for the ω_1 and ω_3 peaks exhibit strong transformations as the excitation energy increases from N-IR excitation to blue excitation, but is most pronounced with excitation energy corresponding to green light; that is $I(\omega_1)$ and $I(\omega_3)$ intensities becoming inversely related with a fall in the total intensity, $I\Sigma(\omega_1, \omega_3)$

and Γ_{ω_1} and Γ_{ω_3} achieve a maximum in the blue–green excitation region. These are not related to tuning into the band gap frequency for *trans*-(CH)_x that requires much less energy (in the N-IR^{18, 38}), but have been regarded as evidence of the presence of inhomogeneity (disorder) in *trans*-(CH)_x chains.

The disorder is due to a distribution of the electronic energy gaps and their respective frequencies; these are selectively probed via the variation of $\hbar\omega_L$ of RRS process, and result in the shift and broadening of phonon bands.⁷ Major attempts to describe the inhomogeneity of *trans*-(CH)_x via a distribution of chains with varying length of π -electron conjugation⁴⁷ employed a particle-in-the-box⁴⁸ and Hückel-type calculations.⁴⁹ The bi-modal distribution model proposed by Brivio and Mulazzi *et al.*^{8, 16} suggested a double peak distribution to arise from individual contributions of both long and short *trans*-(CH)_x segments that show unequal resonant enhancement at a given excitation energy. The inhomogeneity of *trans*-(CH)_x could also be described employing the distribution of the electron-phonon coupling constant λ , $p(\lambda)$ ^{7, 50} of the amplitude mode (AM) theory proposed by Ehrenfreund *et al.*⁷. When other parameters are fixed, λ determines the Peierls relation for the energy gap $E_g(\lambda) = W \exp(-1/(2\lambda))$ and laser frequencies, ω_L , and where W is the width of the π - band. The maximum for $p(\lambda)$ occurs at $\lambda = \lambda_0$, whereas resonance induced changes in peak position, I and Γ result from the condition $\hbar\omega_L = E_g(\lambda) > E_g(\lambda_0)$. We applied the AM model to study *trans*-(CH)_x inclusions in *a*-C:H and the obtained results yielded λ distribution range from ~0.17 for N-IR to ~0.24 for UV, in good agreement with the AM model. The distribution of λ rises from finite localisation lengths and bond length disorder, consequently AM theoretical calculations indicate that *trans*-(CH)_x segments probed by higher $\hbar\omega_L$ are of shorter π - conjugation lengths and of higher bond disorder. The AM findings are complemented by calculations determining the length of the

segments using Brivio and Mulazzi bi-modal distribution model which offers empirical relations for dependence of the conjugation length (long and short) on the frequency of the ω_1 and ω_3 modes. It was found that the approximate length for both single C–C and double C=C bonds in probed *trans*-(CH)_x segments is no less than 120 bond lengths units at the estimation limit of the model; and to a minimum of approximately 8. Shorter chains are probed by higher excitation energies, as illustrated in Fig. 6.¹⁶

The average chain population is $\sim 25 (\pm 5)$ bond length units owing to the uncertainties given by the Raman fitting and the bimodal distribution model.⁸ All *trans*-(CH)_x chains included in *a*-C:H are highly disordered as evidenced by wide ω_1 and ω_3 Raman peaks reaching their maximum in the blue-green range, shown in Fig. 3(b).

We have calculated the theoretical distribution for $I(\omega_3)/I(\omega_1)$ vs. $\hbar\omega_L$ independent of a given *trans*-(CH)_x chain length using the AM formalism that was previously completed by Ehrenfreund *et al.*⁷ for the visible laser excitation to include N-IR and UV $\hbar\omega_L$. Fitting of ω_1 and ω_3 spectral constituents delivered the inverse relationship between the $I(\omega_3)$ and $I(\omega_1)$ parameters, $I(\omega_3)/I(\omega_1)$ relative to the laser excitation energy as illustrated in Fig. 4 and Fig. 5(b). Figure 7 shows that our experimental results obtained for the varying $\hbar\omega_L$ are in good agreement with the theoretical distribution predicted by the AM model and with Ehrenfreund's experimental data.

The observation of relative intensities of ω_1 and ω_3 bands, $I(\omega_1)$ and $I(\omega_3)$ (Fig. 4), and the theoretical distribution of $I(\omega_3)/I(\omega_1)$ ratio (Fig. 7) relative to $\hbar\omega_L$ evidences that ω_1 and ω_3 peak resonance responses to excitation energy of green laser are essentially equal. These are indicated by equal magnitudes of $I(\omega_1)$ and $I(\omega_3)$

shown in Fig. 4 and the $I(\omega_3)/I(\omega_1)$ ratio approaching 1.0 following the AM calculations graphically represented in Fig. 7. This observation suggest that green Raman laser could become a wavelength of choice for natural identification of *trans*-(CH)_x inclusions in carbonaceous materials fitting both ω_1 and ω_3 contributions at equivalent intensities.

B. Identification of carbyne inclusions in *a*-C:H

The Raman spectra in the range of 1900 – 2200 cm⁻¹ are commonly identified with carbyne species.^{24, 25, 34, 35} Figure 8 shows the RRS of examined *a*-C:H films; the spectra from 532 nm to 325 nm displays only minor perturbations in this range and the *sp* contributions become clearly visible when probed by 244 nm laser.

Stability of polyynes and cumulene (*sp*-bonded) species is greatly influenced by the hydrogen environment, and polyynes are known to be significantly more resistant to hydrogen exposure.²¹ For that reason we consider polyynes to be prevailing species in the studied *a*-C:H. Polyynes have been theoretically predicted^{23, 51} to be more energetically stable than cumulenes, and such preferential stability have been evidenced experimentally.^{22, 52} Recent works by Tabata *et al.*^{53, 54} substantiated the assignment of Raman frequency modes centred at around 2000 cm⁻¹ to hydrogen capped short *H*-(*CC*)_{*n*}-*H* polyynic chains with *n* = 8 – 18, as did other workers on this subject.^{55, 56} The assignment of the peaks at ~1950 cm⁻¹ and 2070 cm⁻¹ which appeared in the 244 nm spectrum to fixed-length polyynes is unjustified in our case, since the great majority of published work on the subject considers *sp* inclusions as freestanding. Satisfactory explanation for observation of polyynes exclusively under

UV excitation (Fig. 8) could no longer be regarded resulting from the resonance enhancement of apparently smaller cross section area of one dimensional carbyne species, as we considered previously³⁴ relying on D'Urso *et al.*¹⁹ findings which suggested nearly an exponential increase of combined $sp-sp^2$ probing signal with respect to increasing $\hbar\omega_L$. Such a relationship was not confirmed when sp -rich hydrogen-free $sp-sp^2$ agglomerates were studied using the RRS over the wide energy range⁵⁷, neither such relationship was found valid for significant sp inclusions in polymeric a -C:H.³¹ The appearance of sp -bonded species under UV excitation (VDOS probing) could be attributed to very short chains of wide band gap, such chains are most likely end-terminated on the sp^2-sp^3 matrix of an a -C:H.

Figure 9 illustrates $C-H$ stretching band spectra in the range of $3400 - 2700 \text{ cm}^{-1}$ taken from a -C:H samples after a baseline correction. The configuration of constituent groups is shown in abbreviated form as: saturated (sat); unsaturated (unsat); aromatic (A); olefinic (O); symmetric (sym); and asymmetric (asym). The quantitative^{5, 6, 32, 58} decomposition reveals contributions from the carbyne species at 3000 cm^{-1} ; the amount of sp -hybridised inclusions estimated using Liu *et al.*³² calculations never exceeded 3 % for all films deposited.

The $trans-(CH)_x$ mode is visible at 2995 cm^{-1} , however the infrared absorption of this mode is expected to be significantly lower than other $C-H$ modes fitted, as compared to free molecules. The relative intensity and FWHM of this mode was found closely related to hydrogen content in the films^{13, 31}; the mode contribution for the films studied was between 7 to 10 %. The stretching mode corresponding to $trans$ -vinylene was found at approximately 3020 cm^{-1} .⁴⁶ The amount of carbyne species in a -C:H was found to some extent related to hydrogen content in the films, the ion

energy during deposition and deposition temperature; the amount of *trans*-(CH)_x and PPV inclusions was strongly influenced by plasma density and electron temperature.³¹

IV. SUMMARY AND CONCLUSIONS

In summary, we have performed the RRS investigation on ICP fabricated *a*-C:H films and have demonstrated that the films host *trans*-(CH)_x segments of various conjugation length, poly(*p*-phenylene vinylene) chains as evidenced by the 1175 cm⁻¹ Raman mode and, a small fraction of carbyne species as evidenced under UV excitations. We provided the theoretical basis for arguing that the RRS response of *trans*-(CH)_x chains in the *a*-C:H matrix to changing Raman excitation energy is identical to that of freestanding chains in bulk *trans*-polyacetylene leading to reliable identification of *trans*-(CH)_x inclusions in *a*-C:H and, differentiation between Raman active modes for *trans*-(CH)_x and PPV in *a*-C:H. We observed that relative intensities of *trans*-(CH)_x core A_g modes (ω_1 and ω_3) are essentially equal when probed by excitation energy of green light laser. This is although supported by the theoretical distribution of $I(\omega_3)/I(\omega_1)$ ratio relative to Raman excitation energy, overall exemplifying the approach for *trans*-(CH)_x identification in carbonaceous solids.

The length of *trans*-(CH)_x segments in the films examined was found averaging ~25 (\pm 5) C=C bond length units, with longer chains of up to 120 bond length units probed by N-IR and shorter chains of ~8 units probed by UV $h\omega_L$; all *trans*-(CH)_x inclusions irrespective of conjugation length displayed high degree of bonding disorder. We assigned the 1175 cm⁻¹ peak to PPV CC-H bending mode of the ring and postulated the origin of this mode. *Sp*-hybridised species observed exclusively

under UV excitation were identified as very short polyynic chains of wide band gap, and assumed to be end-terminated on the sp^2 - sp^3 matrix of an a -C:H.

The presence of carbyne, $trans$ -(CH)_x inclusions and $trans$ -vinylene segments was confirmed by complimentary FT-IR analysis.

Finally, the inclusions of basic polymeric chains such as long $trans$ -(CH)_x and PPV were possible owing to highly ordered sp^2 host component of a -C:H films. Such sp^2 ordering was achieved via fabrication of a -C:H films in ICP reactor with high plasma density and low electron temperature compared to conventional DLC deposition systems. A parallel could be drawn with the report by Chen *et al.*⁵⁹ where unusual inclusions of silicon based spherical nanocrystallites into DLC matrix was possible due to similar ICP fabrication conditions, whereas the stability of carbyne species in a -C:H could be attributed to relatively low temperature deposition process.

ACKNOWLEDGEMENTS

The authors are thankful to G. Hope of Griffith University and S. Praver of the University of Melbourne for assisting with the UV Raman measurements. M.R. is grateful to L. Ravagnan and P. Milani of the University of Milan and members of the Laboratorio Getti Molecolari for valuable discussions. M.R. acknowledges the BAM for the visiting postdoctoral fellowship funding. This work has been supported by the Australian Research Council and Australian Nano TAP program.

REFERENCES

* Electronic address: m.rybachuk@qut.edu.au

- ¹ M. Bernasconi, M. Parrinello, G. L. Chiarotti, P. Focher, and E. Tosatti, *Phys. Rev. Lett.* **76**, 2081 (1996).
- ² G. A. Arbuckle, A. G. MacDiarmid, S. Lefrant, T. Verdon, E. Mulazzi, G. P. Brivio, X. Q. Yang, H. S. Woo, and D. B. Tanner, *Phys. Rev. B* **43**, 4739 (1991).
- ³ J. Robertson, *Mat. Sci. Eng. R* **37**, 129 (2002).
- ⁴ T. López-Ríos, É. Sandré, S. Leclercq, and É. Sauvain, *Phys. Rev. Lett.* **76**, 4935 LP (1996).
- ⁵ B. Dischler, A. Bubenzer, and P. Koidl, *Solid State Commun.* **48**, 105 (1983).
- ⁶ F. Piazza, A. Golanski, S. Schulze, and G. Relihan, *Appl. Phys. Lett.* **82**, 358 (2003).
- ⁷ E. Ehrenfreund, Z. Vardeny, O. Brafman, and B. Horovitz, *Phys. Rev. B* **36**, 1535 LP (1987).
- ⁸ G. P. Brivio and E. Mulazzi, *Phys. Rev. B* **30**, 876 (1984).
- ⁹ A. Ferrari and J. Robertson, *Phys. Rev. B* **63**, 121405 (2001).
- ¹⁰ R. Pfeiffer, H. Kuzmany, P. Knoll, S. Bokova, N. Salk, and B. Gunther, *Diamond Rel. Mat.* **12**, 268 (2003).
- ¹¹ H. Kuzmany, R. Pfeiffer, N. Salk, and B. Gunther, *Carbon* **42**, 911 (2004).
- ¹² S. Michaelson, O. Ternyak, A. Hoffman, and Y. Lifshitz, *Appl. Phys. Lett.* **89**, 131918 (2006).
- ¹³ K. Teii, T. Ikeda, A. Fukutomi, and K. Uchino, *J. Vac. Sci. Technol. B* **24**, 263 (2006).
- ¹⁴ M. Rybachuk, A. Hu, and J. M. Bell, *Appl. Phys. Lett.* **93**, 051904 (2008).

- ¹⁵ E. Mullazzi, G. P. Brivio, E. Faulques, and S. Lefrant, *Solid State Commun.* **46**, 851 (1983).
- ¹⁶ G. P. Brivio and E. Mulazzi, *Chem. Phys. Lett.* **95**, 555 (1983).
- ¹⁷ A. C. Ferrari and J. Robertson, *Phys. Rev. B* **64**, 075414 (2001).
- ¹⁸ A. J. Heeger, S. Kivelson, J. R. Schrieffer, and W.-P. Su, *Rev. Mod. Phys.* **60**, 781 LP (1988).
- ¹⁹ L. D'Urso, G. Compagnini, and O. Puglisi, *Carbon* **44**, 2093 (2006).
- ²⁰ R. B. Heimann, J. Kleiman, and N. M. Salansky, *Nature (London)* **306**, 164 (1983).
- ²¹ C. Lenardi, E. Barborini, V. Briois, L. Lucarelli, P. Piseri, and P. Milani, *Diamond Rel. Mat.* **10**, 1195 (2001).
- ²² R. G. Agostino, T. Caruso, G. Chiarello, A. Cupolillo, D. Pacile, R. Filosa, V. Formoso, E. Colavita, L. Papagno, C. Ducati, E. Barborini, C. Lenardi, G. Bongiorno, P. Piseri, and P. Milani, *Phys. Rev. B* **68**, 035413 (2003).
- ²³ M. Springborg and L. Kavan, *Chem. Phys.* **168**, 249 (1992).
- ²⁴ L. Ravagnan, F. Siviero, C. Lenardi, P. Piseri, E. Barborini, P. Milani, C. S. Casari, A. L. Bassi, and C. E. Bottani, *Phys. Rev. Lett.* **89**, 285506 (2002).
- ²⁵ A. Hu, M. Rybachuk, Q. B. Lu, and W. W. Duley, *Appl. Phys. Lett.* **91**, 131906 (2007).
- ²⁶ A. Hu, S. Griesing, M. Rybachuk, Q.-B. Lu, and W. W. Duley, *J. Appl. Phys.* **102**, 074311 (2007).
- ²⁷ R. B. Heimann, *Diamond Rel. Mat.* **3**, 1151 (1994).
- ²⁸ R. H. Baughman, *Science* **312**, 1009 (2006).
- ²⁹ I. K. Varga, *J. Vac. Sci. Technol. A* **7**, 2639 (1989).
- ³⁰ M. Rybachuk and J. M. Bell, *Diamond Rel. Mat.* **15**, 977 (2006).
- ³¹ M. Rybachuk, A. Hertwig, M. Weise, M. Sahre, and U. Beck, (to be published).

- ³² S. Liu, S. Gangopadhyay, G. Sreenivas, S. S. Ang, and H. A. Naseem, *Phys. Rev. B* **55**, 13020 (1997).
- ³³ C. Casiraghi, A. C. Ferrari, and J. Robertson, *Phys. Rev. B* **72**, 085401 (2005).
- ³⁴ A. Hu, Q.-B. Lu, W. W. Duley, and M. Rybachuk, *J. Chem. Phys.* **126**, 154705 (2007).
- ³⁵ A. Hu, M. Rybachuk, Q.-B. Lu, and W. W. Duley, *Diamond Rel. Mat.* **17**, 1643 (2008).
- ³⁶ S. Praver, K. W. Nugent, Y. Lifshitz, G. D. Lempert, E. Grossman, J. Kulik, I. Avigal, and R. Kalish, *Diamond Rel. Mat.* **5**, 433 (1996).
- ³⁷ D. C. Benner, C. P. Rinsland, V. M. Devi, M. A. H. Smith, and D. Atkins, *J. Quant. Spectrosc. Radiat. Transfer* **53**, 705 (1995).
- ³⁸ G. P. Brivio and E. Mulazzi, *Phys. Rev. B* **30**, 876 (1984).
- ³⁹ D. B. Fitchen, *Mol. Cryst. Liq. Cryst.* **83**, 95 (1982).
- ⁴⁰ H. Kuzmany, *Phys. Status Solidi B* **97**, 521 (1980).
- ⁴¹ G. Lanzani, S. Luzzati, R. Tubino, and G. Dellepiane, *J. Chem. Phys.* **91**, 732 (1989).
- ⁴² E. Mulazzi, *Solid State Commun.* **55**, 807 (1985).
- ⁴³ M. Baitoul, J. Wery, J.-P. Buisson, G. Arbuckle, H. Shah, S. Lefrant, and M. Hamdoume, *Polymer* **41**, 6955 (2000).
- ⁴⁴ M. Tzolov, V. P. Koch, W. Bruetting, and M. Schwoerer, *Synthetic Metals* **109**, 85 (2000).
- ⁴⁵ I. Orion, J.-P. Buisson, and S. Lefrant, *Physical Review B* **57**, 7050 (1990).
- ⁴⁶ D. D. C. Bradley, *Journal of Physics D: Applied Physics* **20**, 1389 (1987).
- ⁴⁷ L. S. Lichtmann, D. B. Fitchen, and H. Temkin, *Synthetic Metals* **1**, 139 (1980).
- ⁴⁸ H. Kuzmany, *Pure Appl. Chem.* **57**, 235 (1985).

- ⁴⁹ R. Tiziani, G. P. Brivio, and E. Mulazzi, *Phys. Rev. B* **31**, 4015 (1985).
- ⁵⁰ Z. Vardeny, E. Ehrenfreund, O. Brafman, and B. Horovitz, *Phys. Rev. Lett.* **51**, 2326 (1983).
- ⁵¹ M. Kertesz, J. Koller, and A. Azman, *J. Chem. Phys.* **68**, 2779 (1978).
- ⁵² C. S. Casari, A. L. Bassi, L. Ravagnan, F. Siviero, C. Lenardi, P. Piseri, G. Bongiorno, C. E. Bottani, and P. Milani, *Phys. Rev. B* **69**, 075422 (2004).
- ⁵³ H. Tabata, M. Fujii, and S. Hayashi, *Chem. Phys. Lett.* **420**, 166 (2006).
- ⁵⁴ H. Tabata, M. Fujii, S. Hayashi, T. Doi, and T. Wakabayashi, *Carbon* **44**, 3168 (2006).
- ⁵⁵ C. S. Casari, A. L. Bassi, A. Baserga, L. Ravagnan, P. Piseri, C. Lenardi, M. Tommasini, A. Milani, D. Fazzi, C. E. Bottani, and P. Milani, *Phys. Rev. B* **77**, 195444 (2008).
- ⁵⁶ L. Ravagnan, G. Bongiorno, D. Bandiera, E. Salis, P. Piseri, P. Milani, C. Lenardi, M. Coreno, M. de Simone, and K. C. Prince, *Carbon* **44**, 1518 (2006).
- ⁵⁷ L. Ravagnan and P. Milani, (to be published).
- ⁵⁸ M. Rybachuk and J. M. Bell, *Thin Solid Films* **515**, 7855 (2007).
- ⁵⁹ L.-Y. Chen and F. C.-N. Hong, *Appl. Phys. Lett.* **82**, 3526 (2003).

FIGURE CAPTIONS

FIG. 1 Resonant Raman spectra of bulk *trans*-(CH)_x at 78 K taken for different laser excitation wavelengths. a) $\omega_L = 457.9$ nm; b) $\omega_L = 514.5$ nm; c) $\omega_L = 600$ nm; d) $\omega_L = 676.4$ nm, adapted from Ref. 15.

FIG. 2 Resonant Raman spectra of *a*-C:H at 293 K showing contributions from *trans*-(CH)_x (ω_1 and ω_3) modes, PPV (1175 cm⁻¹ mode), and DLC (*D*, *G*, and *T* modes). An asymmetric peak visible at N-IR–visible (green) $\hbar\omega_L$ at 950 cm⁻¹ is the second order *Si*, from Ref. 14.

FIG. 3 (a) Peak dispersion, $\Delta\omega$ and (b) peak widths, Γ for all constituent peaks as a function of the laser excitation energy $\hbar\omega_L$, from Ref. 14.

FIG. 4 Changes in the fitted ω_1 , ω_3 and 1175 cm⁻¹ bands (intensity magnified by a factor of 5) relative to the laser excitation energy $\hbar\omega_L$ in the spectra of *a*-C:H. Light dotted line over ω_1 and ω_3 bands denotes the $I(\omega_3)/I(\omega_1)$ trend.

FIG. 5 (a) Evolution of relative intensities of the 1175 cm⁻¹ peak, $I(1175)$ and *trans*-(CH)_x contributions, $I\Sigma(\omega_1, \omega_3)$ and (b) relative intensities of ω_1 , $I(\omega_1)$ and ω_3 , $I(\omega_3)$ peaks as a function of the laser excitation energy $\hbar\omega_L$.

FIG. 6 Calculated absorption spectra from long and short chains constituting *trans*-(CH)_x samples, adopted from Ref. 16.

FIG. 7 The intensity ratio of $I(\omega_3)/I(\omega_1)$ vs. the laser excitation energy $\hbar\omega_L$ for *trans*-(CH)_x inclusions in *a*-C:H. Solid line is a theoretical calculation performed using the amplitude mode formalism.⁷

FIG. 8 Resonant Raman spectra of carbyne (polyyne) segments in *a*-C:H.

FIG. 9 Decomposed IR stretching vibrations spectra of an *a*-C:H film. The constituent bonding groups are: $sp^1(3300)$ CH, $sp^2(3125)$ =C-H unsat/A/asym, $sp^2(3085)$ =CH₂ unsat/O/asym, $sp^2(3050)$ =C-H sat/A/asym, $sp^2(3020)$ *trans*-vinelyne (CH) sat/O/sym, $sp^2(2995)$ *trans*-(CH)_x sat/O/sym, $sp^3(2970)$ -CH₃ sat/O/asym, $sp^2(2950)$ =CH₂ sat/O/asym, $sp^3(2915)$ =CH, =CH₂ sat/O/asym, $sp^3(2870)$ -CH₃ sat/O/sym, $sp^3(2855)$ =CH₂ sat/O/sym.

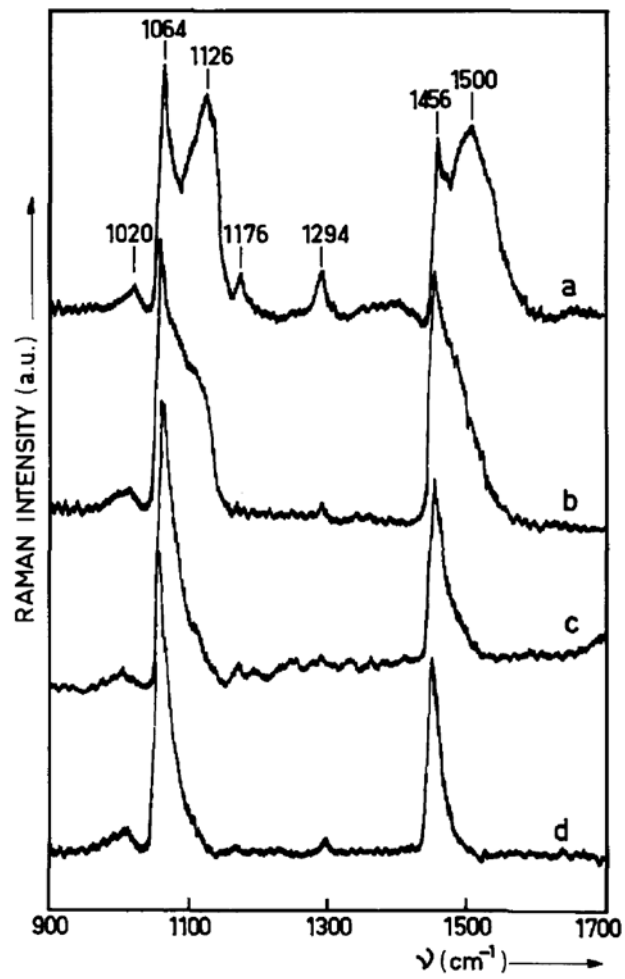


FIGURE 1

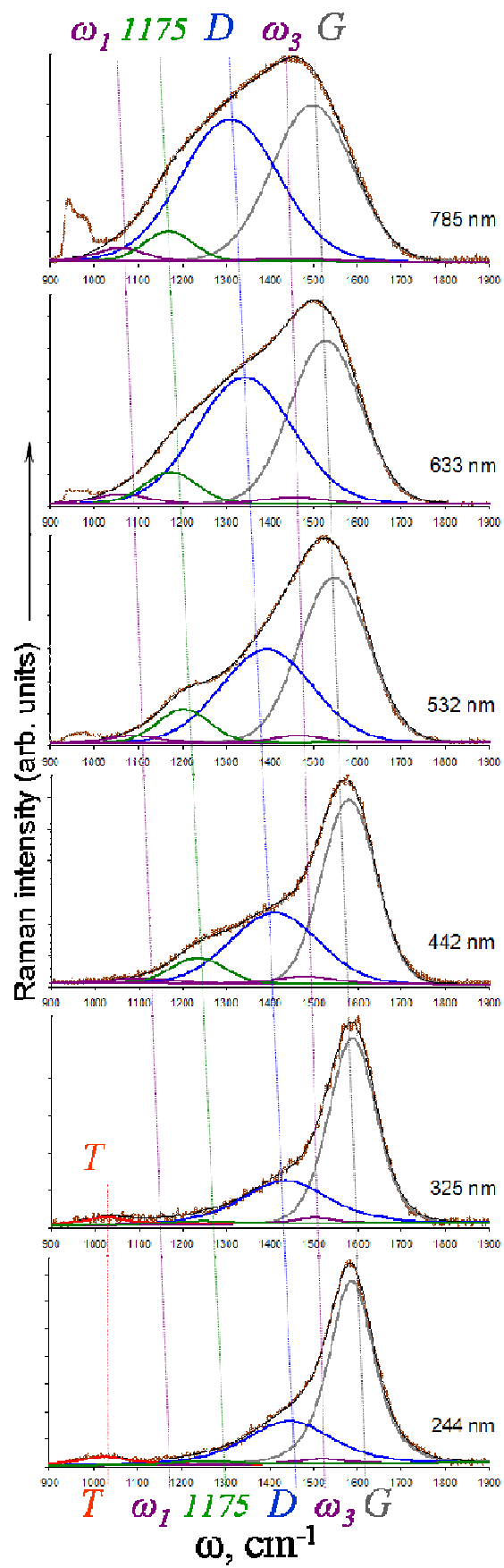


FIGURE 2

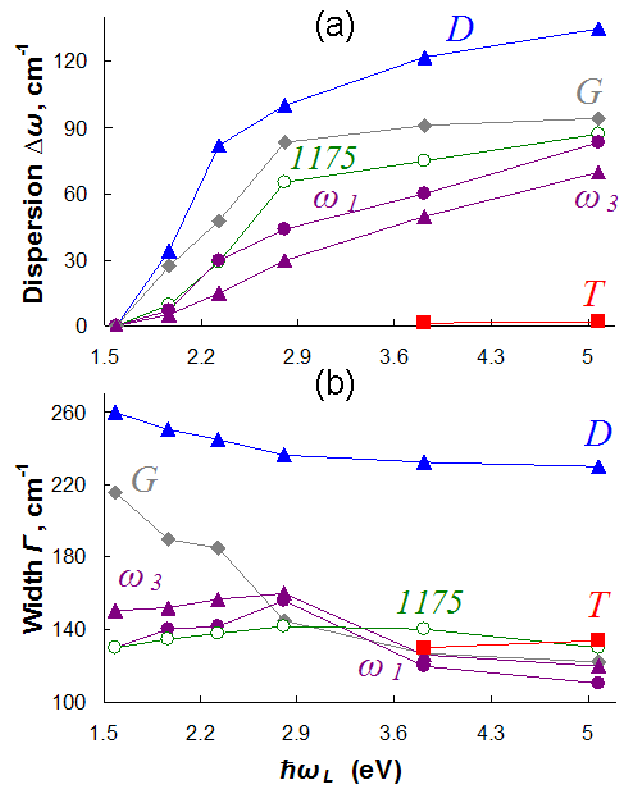


FIGURE 3

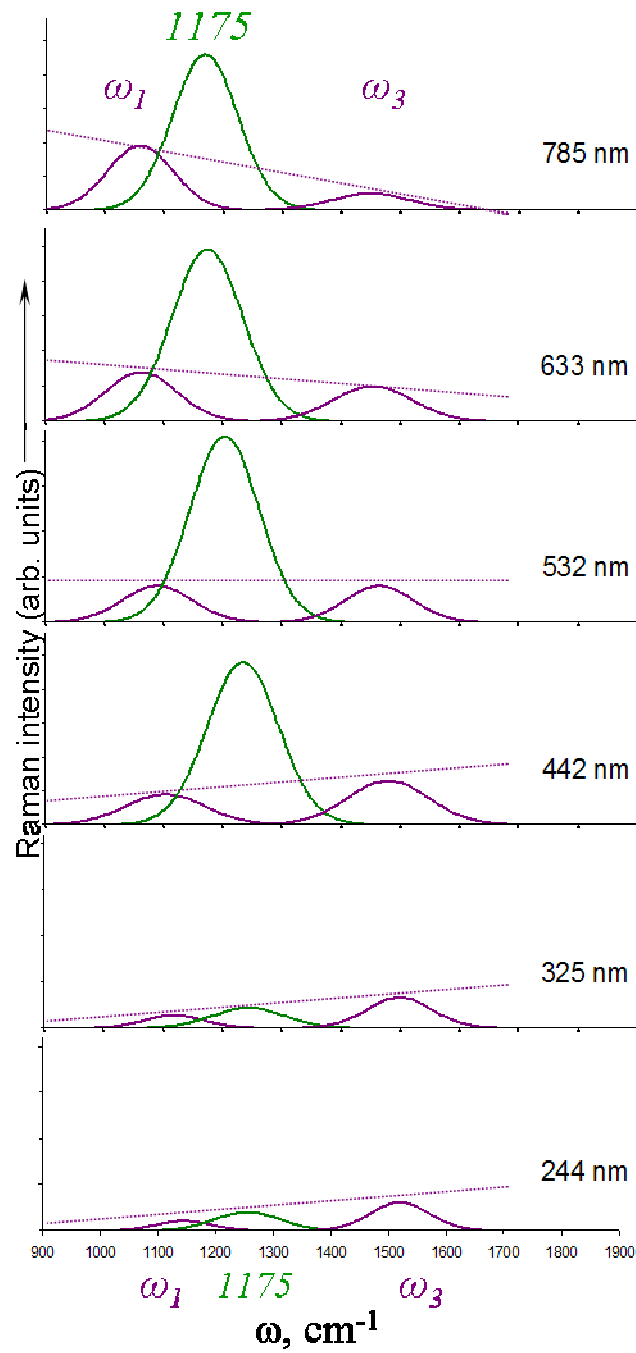


FIGURE 4

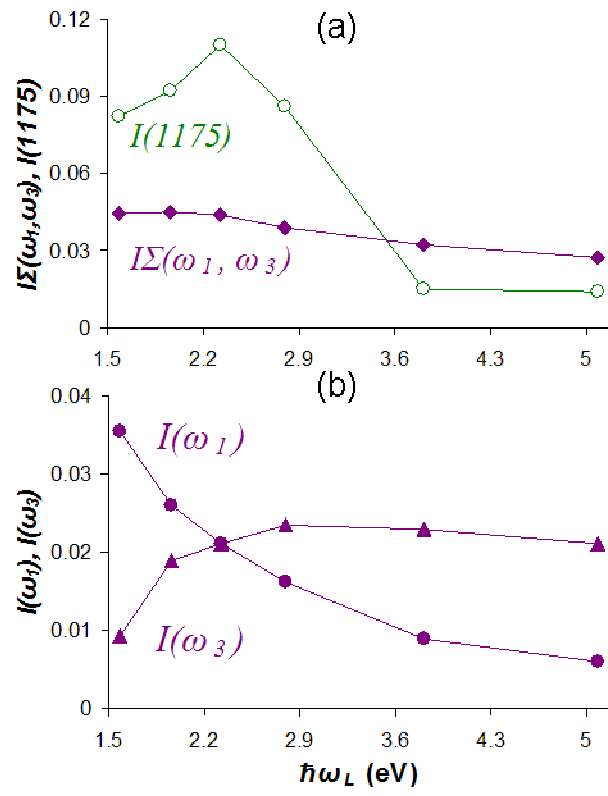


FIGURE 5

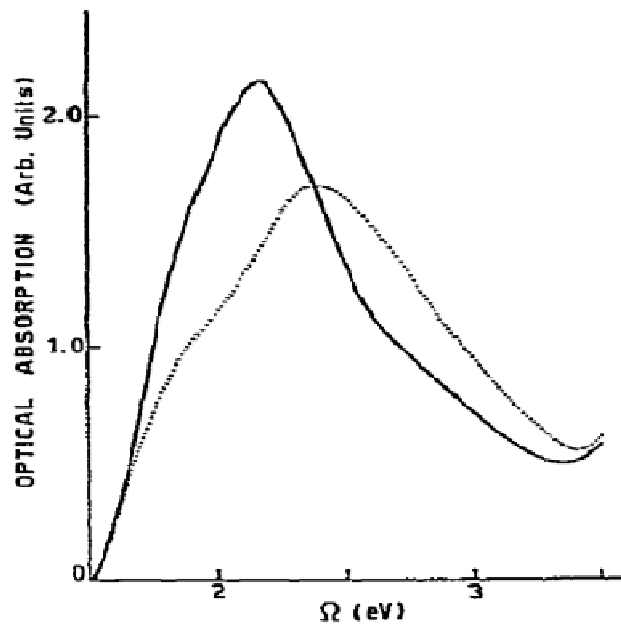


FIGURE 6

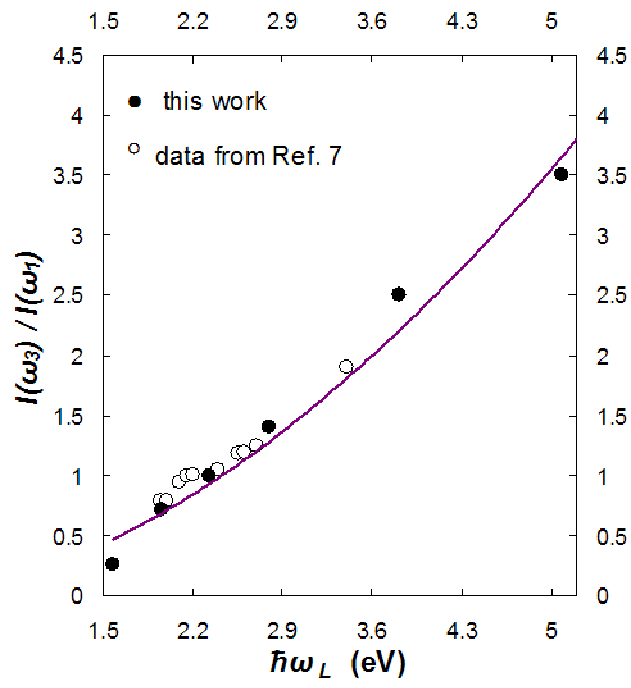


FIGURE 7

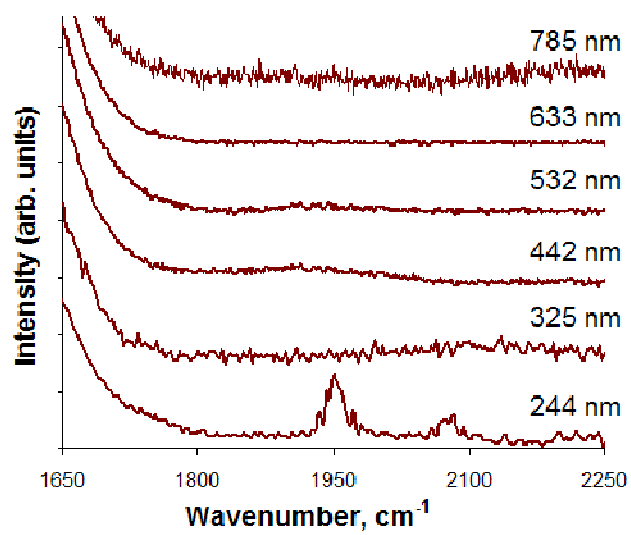


FIGURE 8

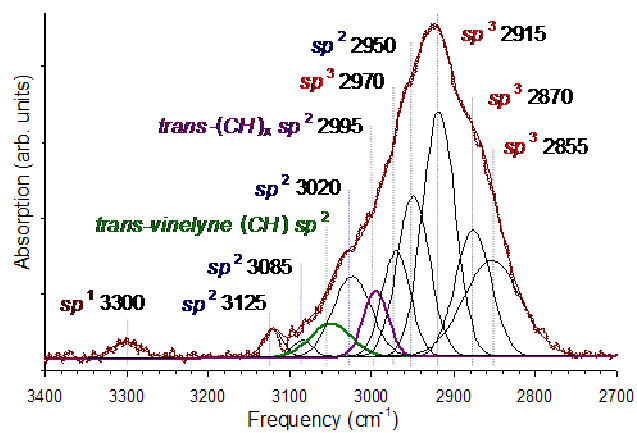


FIGURE 9